ENVIRONMENTAL TECHNOLOGY
2020, VOL. 41, NO. 9, 1127–1138
https://doi.org/10.1080/09593330.2018.1521876

Taylor & Francis
Taylor & Francis Group

Interaction of graphene oxide nanoparticles with quartz sand and montmorillonite colloids

Vasiliki I. Syngouna, Georgios I. Giannadakis and Constantinos V. Chrysikopoulos

School of Environmental Engineering, Technical University of Crete, Chania, Greece

ABSTRACT

Graphene oxide (GO) nanomaterials are used extensively in a wide range of commercial applications. With GO production growing rapidly, it is expected that GO eventually could reach sensitive environmental systems, including subsurface formations, where montmorillonite, one of the most common minerals, is in abundance. This study examines the interaction of GO with quartz sand and montmorillonite (MMT) colloids at pH = 7, ionic strength $I_S = 2$ mM, and 25°C, under dynamic conditions. Moreover, the effect of pH on MMT kinetic attachment onto quartz sand was investigated. The experimental data suggested that pH affected slightly the attachment of MMT colloids onto quartz sand. GO was attached in greater amounts onto MMT than quartz sand. Also, the attachment of GO onto quartz sand was shown to increase slightly in the presence of MMT colloids. However, when GO and MMT coexisted, the total GO mass attached onto quartz sand, suspended MMT, and attached MMT was increased. Furthermore, the equilibrium attachment experimental data were fitted nicely with a Freundlich isotherm, and the attachment kinetics were satisfactorily described with a pseudo-second-order model. Finally, the extended DLVO (XDLVO) theory was used to quantify the various interaction energy profiles based on electrokinetic and hydrodynamic measurements.

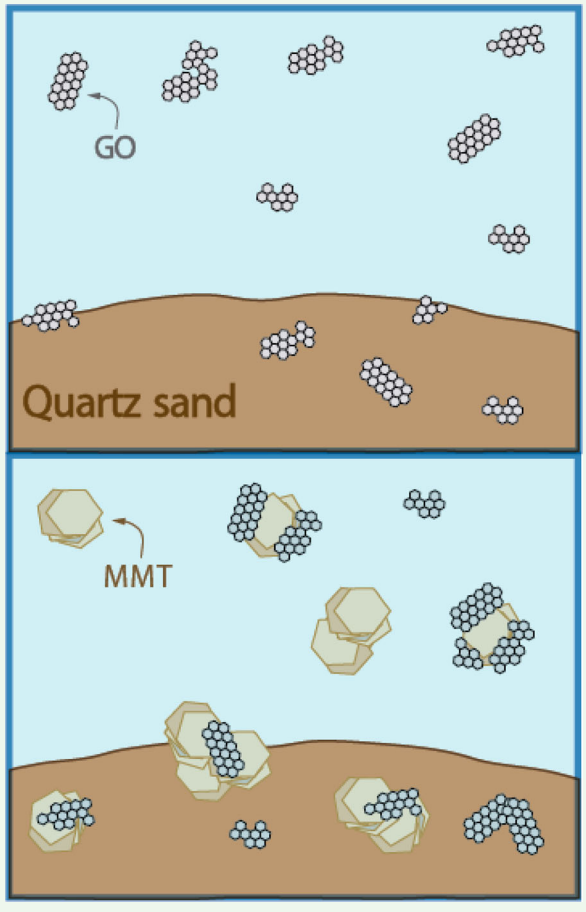

ARTICLE HISTORY
Received 26 March 2018
Accepted 20 August 2018

KEYWORDS
Nanoparticles; graphene oxide; montmorillonite; attachment; quartz sand

CONTACT Constantinos V. Chrysikopoulos cvc@enveng.tuc.gr School of Environmental Engineering, Technical University of Crete, Chania 73100, Greece

1. Introduction

Graphene is a two-dimensional carbon-based nanomaterial with unique physical and chemical properties such as high specific area, high electric and thermal conductivity, gas impermeability, and high mechanical strength [1,2]. One of the most common forms of graphene used in various environmental and medical applications is graphene oxide (GO) [3]. Given the wide use of GO in many different applications, it is almost certain to be released in groundwater systems [4,5]. Clays, are formed by platelets, stacked from a few to as many as one thousand sheets, are natural sorbents for pollutants in the subsurface [6–9]. Montmorillonite, a 2:1 dioctahedral smectite is one of the most ubiquitous aluminosilicate clays in the aquatic environment and primary component of bentonite [10]. Bentonite is often used in technical applications, such as chemical barriers in landfills and toxic waste impoundments.

Several laboratory studies have focused on the transport, stability, and aggregation kinetics of GO over a broad range of environmental conditions (e.g. solution chemistry, GO concentration, flow rate, moisture content, presence of organic matter, and metal oxides) [4,5,11–28]. GO stability was found to be highly dependent on cation valence, ionic strength (I_S) and pH, and less affected by the anion valence [15,16]. Moreover, GO aggregation and deposition in the aquatic environment increased in the presence of metal oxides and natural organic matter [17,19,27]. Furthermore, various investigators have examined the stability of GO due to heteroaggregation with clay minerals such as kaolinite [26,29].

However, although GO has been found highly stable in natural surface waters [15,17], interactions of GO with other environmental surfaces (e.g. clays) could be a major determinant of their fate in the environment. The pH and I_s dependent GO attachment onto kaolinite has previously been investigated [30], but the structure and the chemical composition of kaolinite and montmorillonite are different. Thus, their physical, chemical, and attachment properties are also dissimilar. The various montmorillonite layers have permanent negative charges due to isomorphic substitutions; also, pH-dependent (either positive or negative) charges develop at the edges [31,32]. As a result, montmorillonite colloids can provide favourable attachment surfaces for negatively charged nanomaterials like GO, and could control GO's fate in the environment.

The aim of this study was to investigate the attachment of GO on quartz sand alone and in the co-presence of montmorillonite in PBS solution (pH = 7 and I_S = 2 mM), under dynamic batch conditions. Moreover, the effect of pH, on montmorillonite attachment onto quartz sand was investigated. The GO attachment kinetics and isotherms, related to its interactions with montmorillonite and quartz sand were examined. Also, the attachment of GO onto both montmorillonite and quartz sand was related to theoretically determined extended DLVO (XDLVO) energy interaction profiles, based on electrokinetic and hydrodynamic measurements. To our knowledge, no previous study has focused on the interactions of GO with quartz sand in the presence of montmorillonite colloids. The findings of this study shed some light on the behaviour of GO in environmental systems where common minerals such as montmorillonite are present.

2. Materials and methods

2.1. GO

Graphene oxide stock suspension at a concentration of 20 ppm was prepared by mixing 3 mg of GO sheets (Sigma Aldrich, St. Louis, U.S.A.) with 150 mL of a phosphate buffered solution (PBS) at each solution chemistry (pH and I_S) examined in this study. Afterwards, the GO suspensions were sonicated (37 kHz) (Elmasonic S 30/(H), Elma Schmidbauer GmbH, Singen, Germany) for 2 h for thorough dispersion, as suggested by Sotirelis and Chrysikopoulos [33]. All the solutions were prepared using ultrapure water (Easypure II, Barstead, U.S.A.) with a specific resistivity of ~18.2 MΩ cm at 25°C. The various PBS solutions with different ionic strengths (I_S = 2 and 20 mM at pH 7) were prepared with different amounts of NaCl (C_{NaCl} = 0, and 18 mM); whereas, the PBS solution with different pH values (pH = 4, 7, 10 at I_S = 2 mM) were adjusted with a small amount of either HCl or NaOH solution, which had negligible effect on the solution I_S. The concentration of GO used in all batch experiments was C_{GO} = 5 ppm. The optical density of the GO was analysed at the optimal wavelength of 231 nm by a UV–visible spectrophotometer (Cary 400 BIO, Varian, Palo Alto, California) following the procedure outlined by Liu et al. [13]. Calibration curves were prepared for each set of solution chemistry (pH and I_S) examined in this study, in order to establish the relationship between absorbance, Abs [–], and GO concentration in the range 1–20 ppm.

2.2. Montmorillonite (MMT)

The montmorillonite (STx-1b, Ca-rich montmorillonite, Gonzales County, Texas) used in this study was purchased from the Clay Minerals Society (Columbia, Missouri, U.S.A.). MMT had a specific surface area (SSA) of 82.9 m^2/g [34], as evaluated by the Brunauer–Emmet–Teller (BET) method, and a high cation exchange capacity (CEC) of 84.4 meq/100 g [35]. The <2 μm colloidal

fraction, used in all of the experiments conducted in this study, was separated by sedimentation following the procedures outlined by Rong et al. [36]. The size of the MMT colloids was confirmed using a Zetasizer (Nano ZS90, Malvern Instruments, Southborough, MA). The desired MMT suspensions were prepared by adding an appropriate amount of MMT to PBS at the desired solution chemistry (pH and I_S) and sonicating for 30 min. The concentration of MMT colloids used in all batch experiments was $C_{MMT} = 100$ ppm and was determined by a UV–visible spectrophotometer (Cary 400 BIO, Varian, Palo Alto, California) at a wavelength of 280 nm. Calibration curves were prepared for each set of solution chemistry (pH and I_S) examined in this study, in order to establish the relationship between absorbance, Abs [–], and MMT, in the range 10–150 ppm.

2.3. Quartz sand

Quartz sand (Filcom, Netherlands) with grain diameter ranging from 0.425 to 0.600 mm (sieve no. 40) was used in this study. The sand was washed sequentially by tap water, 0.1 M nitric acid HNO_3 (70%) for 3 h, rinsed with ddH_2O, then soaked in 0.1 M NaOH for 3 h, and rinsed with ddH_2O again [37,38] to remove metal oxides and other impurities following the procedures outlined by Chrysikopoulos and Aravantinou [39]. Finally, the quartz sand was dried in an oven at 80°C.

2.4 Electrokinetic and hydrodynamic measurements

Various electrokinetic and hydrodynamic properties of GO, MMT and quartz sand were determined under various PBS solution chemistries including various ionic strength ($I_S = 2$ and 20 mM at pH 7), and pH (pH = 4, 7, 10 at $I_S = 2$ mM) values at 25°C. The hydrodynamic diameter (d_H) and zeta potential (ζ-potential) of GO were measured with a zetasizer. Note that the ζ-potentials of the quartz sand under various solution chemistry conditions were determined following the methodology described by Mitropoulou et al. [40]. All ζ-potential and d_H measurements were obtained in triplicates and the measurements are listed in Table 1.

2.5. Aggregation kinetics

The kinetics of MMT and GO aggregation, under the experimental conditions, were investigated with the procedure developed by Zhou et al. [41]. Time-resolved hydrodynamic size data of the various MMT and GO suspensions in PBS were measured using dynamic light scattering (DLS) (Nano ZS90, Malvern Instruments, Southborough, MA). The size of MMT and GO aggregates was estimated at various time intervals for the experimental period of 240 min. All DLS measurements were obtained at 25°C.

2.6. Batch experiments

Three sets of dynamic batch experiments were conducted in PBS solution ($I_S = 2$ mM, pH = 7) at 25°C, in order to examine the attachment of MMT onto quartz sand and the attachment of GO onto both MMT and quartz sand. Moreover, the effect of pH on MMT kinetic attachment onto quartz sand was investigated. All sets of experiments were performed in 20 mL Pyrex glass screw-cap tubes (Fisher Scientific). For the first set of experiments of MMT attachment onto quartz sand, 16 glass tubes were employed, which were divided into two groups. The first group of glass tubes (reactor tubes) contained 14 mL of MMT suspension with 14 g of sand and the second group of glass tubes (control tubes) contained 20 mL of MMT suspension without sand in order to monitor possible MMT aggregation and attachment onto the tube walls. For the second set of experiments and GO attachment onto quartz sand, 16 glass tubes were employed, which were divided into two groups. The first group of glass tubes (reactor tubes) contained 14 mL of GO suspension with 14 g of sand and the second group of glass tubes (control tubes) contained 20 mL of GO suspension without quartz sand in order to monitor possible GO aggregation and attachment onto the tube walls. For the third set of experiments and GO attachment onto both MMT and quartz sand, 16 glass tubes were employed, which were also divided into two groups. The first group of glass tubes

Table 1. Measured zeta potentials and hydrodynamic diameters of GO, MMT and quartz sand.

Experimental conditions			GO		MMT		Quartz sand
pH	I_S (mM)	T (°C)	ζ-potential (mV)	d_H (nm)	ζ-potential (mV)	d_H (nm)	ζ-potential (mV)
7	2	25	−40.9	351.4	−32.9	1332	−27
7	20	25	−43.1	829	−41.9	1804	na[†]
4	2	25	−32.1	4325	−27.1	1129	−23.6
10	2	25	−48.1	511.7	−40.9	1826	−38.5

[†]Values are not available.

(reactor tubes) contained 7 mL of GO suspension and 7 mL of MMT suspension with 14 g of sand and the second group of glass tubes (control tubes) contained 10 mL of GO suspension and 10 mL of MMT suspension without sand in order to monitor GO–MMT heteroaggregation and possible GO attachment onto both MMT and tube walls. Furthermore, eight glass tubes (blank tubes), which contained only 14 mL of PBS and 14 g of sand, were also employed as blanks. All glass tubes were filled to the top. In each set of experiments, the various tubes were treated in the same manner.

For the first set of kinetic attachment experiments, a sample (3.0 mL) was removed from each selected glass tube at different preselected times (0, 5, 10, 20, 30, 60, 120, 180, 240 min) and the corresponding MMT concentration was measured. The concentrations of MMT attached onto quartz sand were then calculated by mass difference. All used glass tubes were discarded. For the second and third sets of kinetic attachment experiments, extra subsamples (2.0 mL) were withdrawn at each time interval and then centrifuged at 3500 rpm for 30 min to remove MMT colloids from GO suspension following the procedure as outlined by Zhao et al. [29]. Note that after centrifugation, 1.5 mL of the supernatant was carefully moved to another 2 mL centrifuge tube and the GO concentration in the supernatant was determined. The concentration of the attached GO onto MMT and quartz sand was then calculated by mass difference. Note that for the equilibrium attachment experiments different initial MMT (25, 50, 100, 125, 150 ppm) and GO (2, 5, 7, 10, 15, 20 ppm) concentrations were employed. A schematic illustration of the experimental procedures is presented in Figure 1.

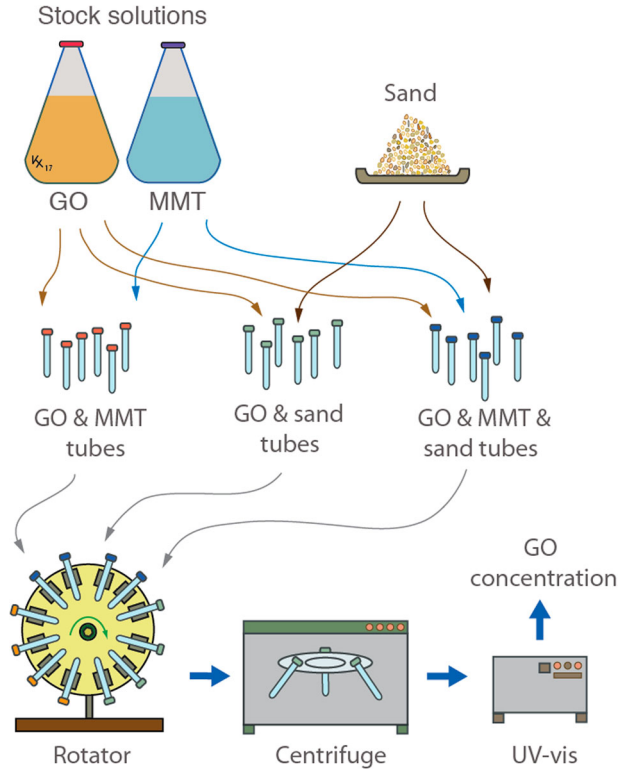

Figure 1. A schematic illustration of the experimental procedures.

2.7. Attachment kinetics

Recent studies suggested that the kinetics of GO attachment onto suspended clay colloids and quartz sand could be described with a pseudo-second-order model [30,33]. Sotirelis and Chrysikopoulos [33] shown that the experimental data of GO attachment onto quartz sand exhibited substantial surface heterogeneity and that GO retention was associated with physicochemical interactions such as chemisorption [42]. Furthermore, thermodynamic analysis revealed that the GO attachment process was nonspontaneous and endothermic, which may be associated with structural changes of the sand surfaces due to chemisorption [33]. Consequently, the kinetic batch data from the MMT and GO attachment experiments were expected to follow a pseudo-second-order equation [30,33,42,43]:

$$\frac{dC_t^*}{dt} = k_{p2}(C_{eq}^* - C_t^*)^2 \quad (1)$$

where t [t] is time; C_t^* [M_p/M_s] is the attached concentration of MMT or GO particles at time t, in units [mg/g]; C_{eq}^* [M_p/M_s] is the attached concentration of MMT or GO particles at equilibrium, in units [mg/g]; and k_{p2} [$M_s/(M_p{\cdot}t)$] is the rate constant of the pseudo-second-order attachment process, in units [g/(mg·min)]. Note that M_p was introduced for the mass of MMT or GO particles, and M_s for the mass of solids (quartz sand or MMT). Separating variables and integrating over time from 0 to t, and the attached particle concentration from 0 to C_t^* yields the following equation:

$$C_t^* = \frac{(C_{eq}^*)^2 k_{p2} t}{1 + C_{eq}^* k_{p2} t} \quad (2)$$

which can also be written in the following linear form:

$$\frac{t}{C_t^*} = \frac{1}{k_{p2}(C_{eq}^*)^2} + \frac{t}{C_{eq}^*} \quad (3)$$

The various MMT or GO kinetic attachment experimental data were fitted with the nonlinear least squares regression software 'ColloidFit' [44].

2.8. Attachment isotherms

The batch data from the equilibrium attachment of MMT and GO particles where fitted with the Freundlich isotherm equation [45]:

$$C^*_{eq} = K_f C^m_{eq} \quad (4)$$

which can be written in the following linear form:

$$\log C^*_{eq} = \log K_f + m \log C_{eq} \quad (5)$$

where C_{eq} [M_p/L^3] is the aqueous phase concentration at equilibrium, in units of [mg/L]; K_f [$L^{3+m}/M_s M_p^{m-1}$] is the Freundlich constant, in units of [(litre of solution)^m/(g mg^{m-1})]; and m [–] is the Freundlich exponent, which is equal to one for linear attachment. It should be noted that K_f is directly proportional to the sorbent capacity for attachment, and m is a measure of the surface heterogeneity of the sorbent (the smaller its value the higher the surface heterogeneity). The Freundlich parameters K_f and m were estimated by fitting of the log-transformed experimental data log C^*_{eq} versus log C_{eq} with the linearized form of the Freundlich isotherm (Equation (5)), using the software 'ColloidFit' [44].

2.9. XDLVO theory calculations

The extended Derjaguin–Landau–Verwey–Overbeek (XDLVO) theory was used to calculate the total interaction energy (Φ_{XDLVO}), under various values of pH and I_S. For the MMT–(sand grains) and GO–(sand grains) interactions, the sphere–plate model was employed; whereas, for the MMT–MMT, GO–GO, and GO–MMT interactions, the sphere–sphere model was employed. The theory considers the effects of Born repulsion (Φ_{Born}), van der Waals attraction (Φ_{vdW}), electrical double layer repulsion (Φ_{dl}), and Lewis acid–base (Φ_{AB}) interactions [11,13,16,46].

3. Results and discussion

3.1. Electrokinetic and hydrodynamic properties of MMT and GO

The electrokinetic and hydrodynamic characterization of GO and MMT as a function of pH and I_S, were summarized in Table 1. The ζ-potential values of GO, MMT and quartz sand were consistently negative under all the tested experimental conditions, which were in agreement with the results of previous studies under identical conditions [4,13,46]. Electrokinetic measurements showed that the ζ-potential of GO decreased significantly from pH 4 to 10 at I_S = 2 mM (from −32.1 to −48.1 mV), while only mild decrease in the ζ-potential of GO was observed by increasing I_S from 2 to 20 mM at pH = 7 (from −40.9 to −43.1 mV) (see Table 1). These results are consistent with other reported studies [15,47]. Moreover, the ζ-potential of GO showed little change with increasing I_S above its critical coagulation concentration (CCC) [26,30]. Also, the ζ-potential of MMT decreased significantly from pH 4 to 10 at I_S = 2 mM (from −27.1 to −40.9 mV) (see Table 1), a trend that has also been observed by other investigators [48]. It is worthy to note that, montmorillonite is a swelling-smectite clay that possesses permanent negative charges on the basal planes due to isomorphic substitution of the Si and Al ions in its structure, as well as conditional charges on amphoteric edge sites (mainly, Si–OH and Al–OH) [49,50]. Moreover, the pH of isoelectric point (or point of zero charge), pH_{IEP}, of the edge groups on montmorillonite is estimated at ~6.5 [31,51]. Therefore, dissociation of surface hydroxyl groups at edge sites is expected to occur when pH > 6.5, contributing more net negative surface charges to the ζ-potential measurement. Furthermore, the ζ-potential of MMT was shown to decrease when I_S was increased from 2 to 20 mM at pH 7 (from −32.9 to −43.1 mV) (see Table 1).

The hydrodynamic diameter values of GO and MMT as a function of pH and I_S were also presented in Table 1. The d_H of GO increased considerably from pH 7 to 10 at I_S = 2 mM (from 350 to 512 nm), while the d_H of GO increased sharply as the pH decreased from 7 to 4 at I_S = 2 mM. The observed increase of GO d_H (>4000 nm) at pH = 4 suggests that the GO suspension is unstable near to its isoelectric point (IEP), due to the reduction in the electrostatic repulsive forces between GO particles, as predicted by the colloidal theory [52]. The pH_{IEP} of graphene was reported to be around 3.8 to 4.7, and for GO $pH_{IEP} \leq 3$ [53]. However, the pH_{IEP} of GO has been reported to increase up to 7.5 by non-covalent electrochemical attachment [54,55]. Also, Note that as the pH decreases, the carboxyl groups, that are presumably located at the edges of the GO nanosheets, are increasingly protonated, which results in less hydrophilic GO nanosheets and GO aggregation [56]. For the experimental conditions of this study (pH = 7 and I_S = 2 mM), the GO was found to be quite stable over time. In the pH range of aquatic environments (4.7 < pH < 9.2) the d_H of GO was found by other investigators to remain relatively steady [15,16,26,57]. Moreover, the d_H of GO was observed to increase significantly with the increase of I_S from 2 to 20 mM at pH = 7 (from 351.4 to 829 nm, see Table 1). In agreement to our observations, the I_S was reported by other investigators to play a significant role on both the ζ-potential and d_H of GO [12,15]. The d_H of MMT at pH = 7 was observed to increase significantly with the increase of I_S from 2 to 20 mM (from 1129 to 1804 nm), while at I_S = 2 mM the d_H of MMT was observed to increase significantly with the increase of pH from 4 to 10 (from 1129 to 1826 nm). However, MMT was found to be quite stable

over time at both pH values examined in this work (pH = 7, 10). Tombácz and Szekeres [31] found that montmorillonite flocculation occurred at pH < pH_{IEP} = 6.5, presumably in the form of edge(+)/face(−) associations when salt concentrations were higher than 10 mM NaCl. On the contrary, in dense suspensions at pH > 6.5 well-ordered lamellar packages occurred. Note that McAtee and Henslee [58] made similar observations. Furthermore, it has been reported that on contact with water, the exchangeable cations of MMT hydrated and the basal sheets expanded under free swelling conditions, depending on the balance of attractive and repulsive forces between the MMT sheets [59]. Note that the swelling pressure was reported to increase with decreasing I_S and increasing pH [60,61]. Therefore, as the pH decreased, the MMT colloids were expected to aggregate and sediment faster. The sedimentation behaviour of MMT in various PBS solutions were shown to be comparable with slopes of falling lines equal to −0.0008, −0.0011, −0.0007 at pH 4, 7 and 10, respectively (see Figure 2).

3.2. Kinetic batch experiments

The attachment of GO onto MMT as a function of contact time was illustrated in Figure 3. The GO kinetic experimental data (PBS solution, pH = 7 and I_S = 2 mM) were fitted with a pseudo-second-order equation, and the fitted kinetic model-parameter-values for k_{p2} and C^*_{eq} were listed in Table 2. The fitting process was performed with the nonlinear least squares regression software ColloidFit [44]. The experimental kinetic data suggested that GO attachment onto MMT was relatively fast, reaching equilibrium within 30 min.

The data from the kinetic batch experiments of GO attachment onto quartz sand (with and without the presence of MMT) as well as the total GO attachment onto both quartz sand and MMT were shown in Figure 4. The fitted parameter values (k_{p2} and C^*_{eq}) for the kinetic model were listed in Table 2. The data from the experiments of GO attachment onto quartz sand in the absence of MMT, under the experimental conditions (PBS solution, pH = 7 and I_S = 2 mM), were presented in Figure 4(a). Note that more GO mass was attached onto MMT (see Figure 3) than onto quartz sand (see Figure 4(a)). Also, the attachment of GO onto quartz sand was shown to be relatively slow, reaching equilibrium within 120 min. Furthermore, the data from the experiments of GO attachment onto quartz sand in the presence of MMT were presented in Figure 4(b). Note that more GO mass was attached onto quartz sand in the presence (see Figure 4(b)) than in the absence (see Figure 4(a)) of MMT, suggesting that GO attachment was facilitated by MMT colloids already attached onto the quartz sand. However, the slightly increased attachment of GO onto sand in the presence of MMT (see Table 2 and Figure 4(b)) was attributed to the competition between MMT and GO for attachment sites on sand surfaces (e.g. metal oxides). The experimental

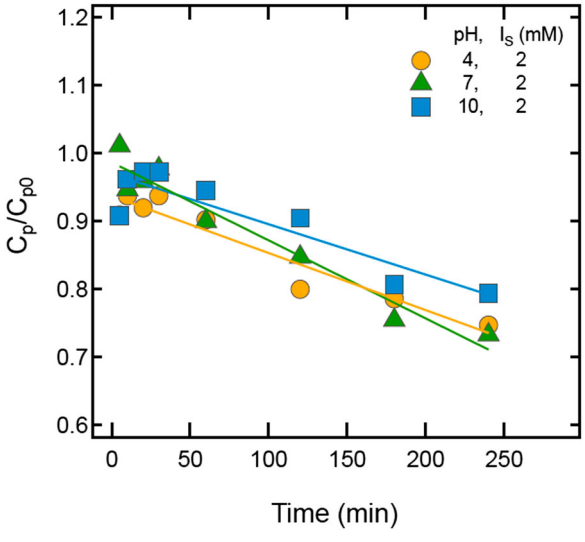

Figure 2. MMT sedimentation under various PBS solutions.

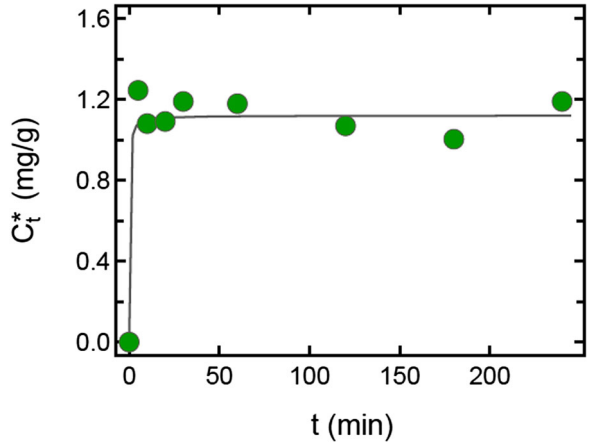

Figure 3. Kinetic attachment of GO onto MMT. The symbols (circles) represent the experimental data and the curve the fitted model simulation. Here, pH = 7, I_S = 2 mM, and T = 25°C.

Table 2. Fitted parameters obtained from the MMT and GO kinetic attachment experiments.

Experimental conditions				
pH	I_S (mM)	T (°C)	C^*_{eq} [mg/g sand]	k_{p2} [g sand/(mg·min)]
MMT onto sand				
7	2	25	0.0271	8.5
10	2	25	0.0233	44.3
GO onto sand				
7	2	25	4.46×10^{-4}	364.8
GO onto MMT				
7	2	25	1.121	5.0
GO onto sand in the presence of MMT				
7	2	25	0.0027	284.1

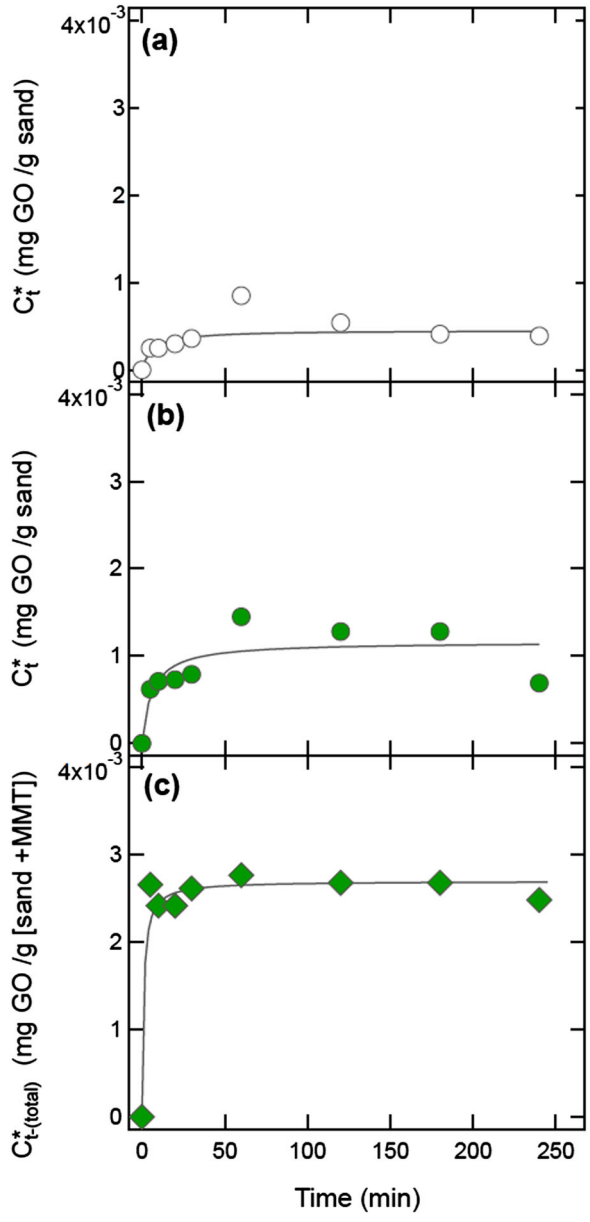

Figure 4. Kinetic attachment of GO onto: (a) quartz sand only, in the absence of MMT (open circles); (b) quartz sand only, in the presence of MMT (solid circles); and (c) the combined mass of quartz sand and MMT (attached and suspended) (solid diamonds). The symbols represent the experimental data and the curves the fitted model simulations. Here, pH = 7, I_S = 2 mM, and T = 25°C.

data of total GO onto both quartz sand and MMT (attached and suspended) were presented in Figure 4 (c), where the attached GO concentration was indicated as $C^*_{t-(\text{total})}$ with units [mg GO/g (sand + MMT)]. Comparison of Figures 4(b) and (c) clearly suggested that more GO was attached onto suspended MMT than MMT already attached onto quartz sand. Note that, in the presence of MMT, GO may alter XDLVO interaction energies between MMT colloids and quartz sand.

The influence of pH on MMT attachment onto quartz sand was shown in Figure 5. The experimental data suggested that there was no significant change in MMT mass attached onto sand grains with increasing pH values from 7 to 10. Furthermore, for all cases examined in this work, the attachment of MMT onto quartz sand was relatively slow, reaching equilibrium within 120 min at pH 7 and within 60 min at pH 10. It should be noted that Yoshida and Suzuki [62] found negligible deposition of montmorillonite colloids onto quartz sand at pH 8 over a 24 h contact period, an observation that was attributable to the negative surface charge of montmorillonite. The average ζ-potential of MMT was about -33.63 ± 6.9 mV at pH 4–10 (see Table 1), a value that is consistent with results of previous studies [62–64]. The negative ζ-potential of the MMT surface at low pH indicated that a permanent negative charge at the tetrahedral sheet was dominant on the surface charge of MMT particle and was independent of the solution physicochemical conditions [65]. Thus, the MMT attachment onto quartz sand was slightly increased with decreasing solution pH (see Figure 5). The observed increase in MMT mass attached onto the quartz sand with decreasing pH values was attributed to the decreasing absolute ζ-potential values with decreasing pH (see Table 1). The fitted kinetic model-parameter-values for k_{p2} and C^*_{eq} were listed in Table 2.

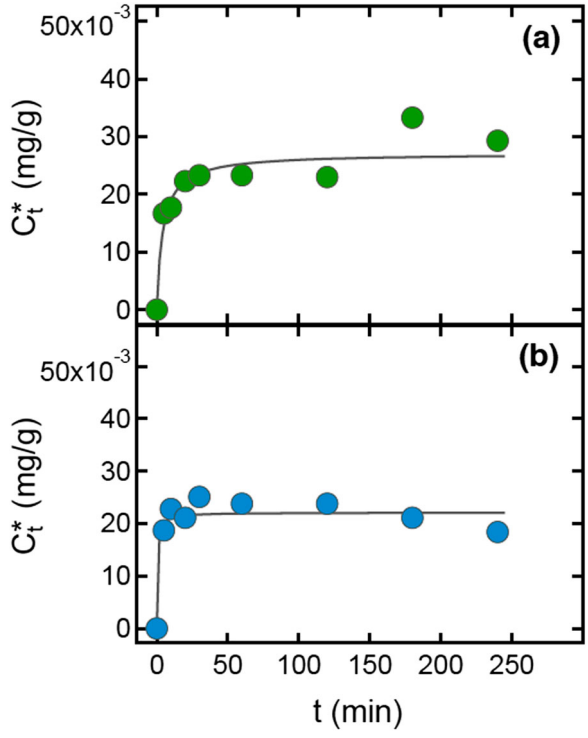

Figure 5. Effect of pH on kinetic attachment of MMT onto quartz sand for: (a) pH = 7, and (b) pH = 10. The symbols (circles) represent the experimental data and the curves the fitted model simulations. Here T = 25°C and I_S = 2 mM.

3.3. Isotherm batch experiments

The equilibrium attachment data for different sorbate/sorbent systems under the experimental conditions (PBS solution, pH = 7, I_S = 2 mM) were presented in Figure 6, and the corresponding Freundlich isotherm parameters were listed in Table 3. Based on the calculated R^2 values (see Figure 6 and Table 3), the Freundlich isotherm model fitted very well the experimental data under the experimental conditions of this study. The attachment of MMT onto quartz sand (Figure 6(a)) and GO onto quartz sand and MMT (Figure 6(b,c)) was a favourable process because all of the estimated m values were less than unity ($m < 1$). Also, the K_f values listed in Table 3 revealed that the sorption affinity of GO for MMT (see Figure 6(c)) was higher than for quartz sand (see Figure 6(b)), and the sorption affinity of MMT was higher than that of GO for quartz sand (see Figure 6(a,b)). Note that, among all sorbate/sorbent combinations examined the strongest aqueous sorption was observed for GO/MMT with sorbent-to-solution distribution coefficient of $K_f = 0.47$ $[L^m/(g)\cdot(mg)^{m-1}]$ (see Table 3).

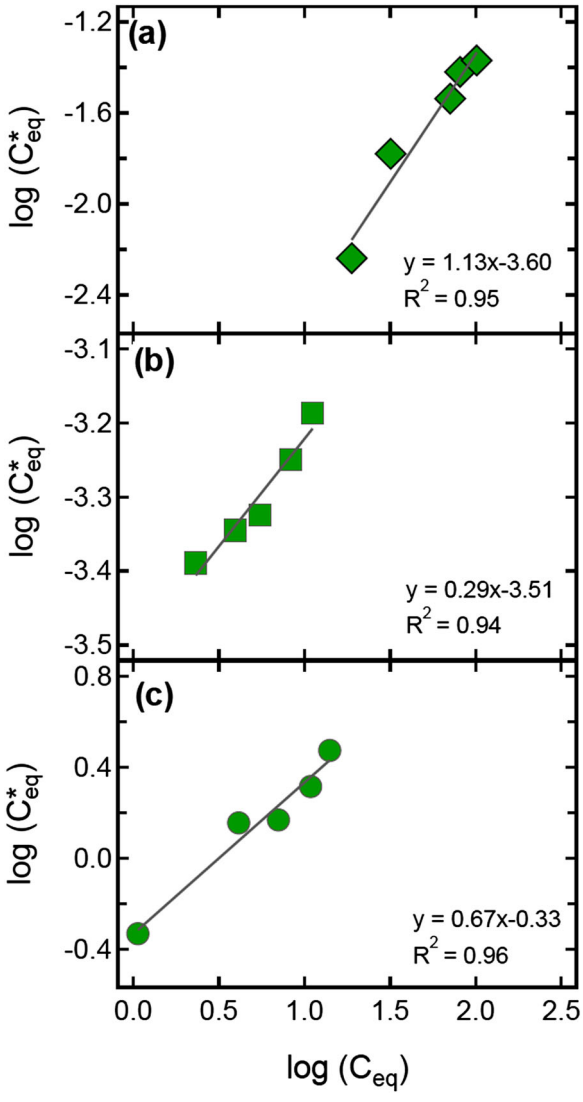

Figure 6. Linearized Freundlich isotherms for the attachment of: (a) MMT onto quartz sand, (b) GO onto quartz sand, and (c) GO onto MMT. The solid lines are the linear regressions with slope equal to m, and the ordinate is equal to logK_f. Here, pH = 7, I_S = 2 mM, and T = 25°C.

3.4. XDLVO results

The Φ_{XDLVO} profiles for GO–quartz sand (see Figure 7(a)) and MMT–quartz sand (see Figure 7(b)) interactions at various pH and I_S conditions for the case of sphere-plate approximation were shown in Figure 7. The Φ_{XDLVO} profiles for GO (see Figure 7(a)) and for MMT (see Figure 7(b)) with sand exhibited a range of energy barriers,

Table 3. Freundlich parameters for GO and MMT equilibrium attachment onto quartz sand for pH = 7 and I_S = 2 mM at 25°C.

Interacting materials	m (–)	K_f $[L^m/(g)(mg)^{m-1}]$	R^2
GO, sand	0.3	3.08×10^{-4}	0.95
MMT, sand	1.1	2.53×10^{-4}	0.94
GO, MMT	0.7	4.66×10^{-1}	0.96

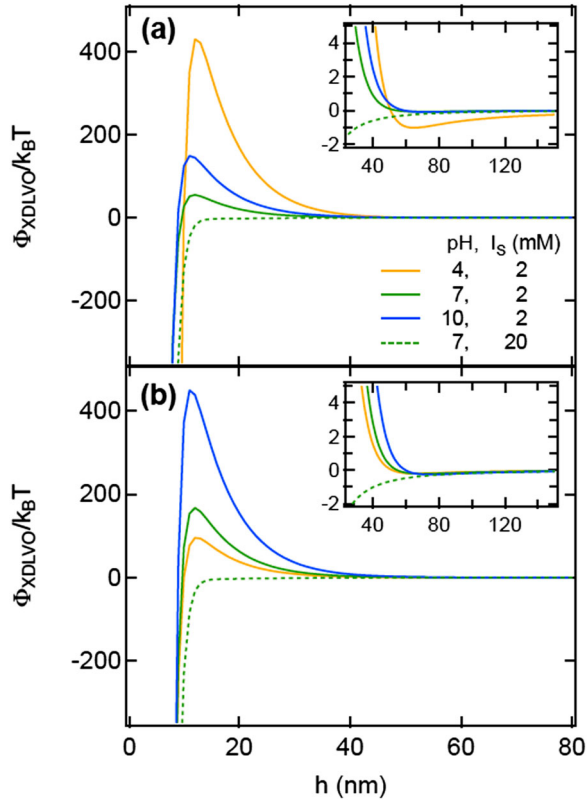

Figure 7. Predicted Φ_{XDLVO} profiles for (a) GO–quartz sand, and (b) MMT–quartz sand interactions, as a function of separation distance for various PBS solutions. Each figure insert highlights the corresponding Φ_{min2}.

Φ_{max1}. Thus, it was almost impossible for both GO and MMT to overcome the imposed Φ_{max1} and to attach onto the sand surfaces in the deep primary minima, Φ_{min1} [66]. However, the XDLVO curves showed the presence of secondary minima, Φ_{min2}, indicating unfavourable attachment (attachment in the Φ_{min2}). The XDLVO calculations for GO-quartz sand interactions presented in Figure 7a and MMT–quartz sand interactions presented in Figure 7(b) shown that the energy barrier (Φ_{max1}) disappeared at $I_S = 20$ mM, indicating that both GO and MMT were deposited in Φ_{min1} (see Table 4). Furthermore, for the evaluation of Lewis acid–base free energy of interaction $\Phi_{AB(h=h_o)}$ [J/m^2] (where h [m] is the separation distance between the approaching surfaces) between GO and quartz sand and MMT and quartz sand at $h = h_o = 0.25$ nm, the Yoon et al. [67] empirical approach was employed. The various $\Phi_{AB(h=h_o)}$ values calculated were listed in Table 5. Worthy to note is that $\Phi_{AB(h=h_o)}$ values were slightly more negative for GO (−3.465 J/m^2) than MMT (−3.027 J/m^2) interactions with quartz sand (see Table 5). These findings are in perfect agreement with the experimental results of this study (see Figure 6 and Table 3), showing that GO attachment was higher than MMT attachment onto quartz sand. Therefore, the XDLVO theory can successfully explain the hydrophobic interaction-mediated attachment of GO and MMT onto quartz sand.

The Φ_{XDLVO} profiles for the case of sphere–sphere approximation, as applied to identical GO-GO, MMT–MMT and GO-MMT interactions at various pH and I_S conditions, were shown in Figure 8. Clearly, the Φ_{XDLVO} curves for both GO–GO (Figure 8(a)) and MMT–MMT (Figure 8(b)) suggested that, for all cases considered, no coagulation between like particles was expected to occur under the experimental conditions. These results confirmed that the GO and MMT suspensions were stable under the experimental conditions, particularly when the I_S was low. However, the XDLVO theory predicted a deep Φ_{min1} of 1575 k_BT for GO–GO case at the experimental conditions of pH = 7 and $I_S = 2$ mM, and suggested that hydrophobic GO–GO interactions could lead to initial GO aggregation. The XDLVO energy profiles for GO-MMT interactions at various pH and I_S conditions were shown in Figure 8(c). Clearly, at high ionic strength of $I_S = 20$ mM the double layer shrinked in size and the GO-MMT interactions were attractive for long distances. Moreover, at $I_S = 2$ mM the deepest Φ_{min2} of 2.837 k_BT was observed at pH = 4 while the lowest Φ_{max1} of 55.09 k_BT at pH = 7. Note that the calculated $\Phi_{AB(h=h_o)}$ value was slightly smaller for GO-GO than MMT–MMT and GO–MMT (see Table 5) and suggested that hydrophobic interactions played an important role on GO attachment onto MMT.

Table 5. Calculated values of $\Phi_{AB(h=h_o)}$ (PBS solution, pH = 7, I_S = 2 mM).

Interacting materials	$\Phi_{AB(h=h_o)}$ (mJ/m^2)
GO–Quartz sand	-3.47×10^3
MMT–Quartz sand	-3.03×10^3
GO–GO	-3.01×10^3
MMT–MMT	-2.30×10^3
GO–MMT	-2.63×10^3

Table 4. Calculated Φ_{max1}, Φ_{min1}, and Φ_{min2} values for sphere–plate and sphere–sphere models using XDLVO theory.

Conditions pH, I_S (mM)	H (nm)	Φ_{min1} (k_BT)	H (nm)	Φ_{max1} (k_BT)	H (nm)	Φ_{min2} (k_BT)
GO–Quartz sand (Sphere–plate)						
4, 2	0.25	-1.13×10^7	12	429	65	−1.033
7, 2	0.25	-9.17×10^5	12	54.9	69	−0.077
10, 2	0.25	-1.34×10^6	11	148.2	73	−0.099
7, 20	0.25	-2.16×10^6	na[a]	na[a]	na[a]	na[a]
MMT–Quartz sand (Sphere–plate)						
4, 2	0.25	-2.57×10^6	12	94.8	66	−0.201
7, 2	0.25	-3.04×10^6	12	167.0	69	−0.220
10, 2	0.25	-4.16×10^6	11	449.7	74	−0.265
7, 20	0.25	-4.11×10^6	na[a]	na[a]	na[a]	na[a]
GO–GO (Sphere–sphere)						
4, 2	na[a]	na[a]	na[a]	na[a]	102	−1.813
7, 2	5	−1575	11	49.1	61	−0.381
10, 2	na[a]	na[a]	na[a]	na[a]	65	−0.503
7, 20	na[a]	na[a]	na[a]	na[a]	31	−1.275
MMT–MMT (Sphere–sphere)						
4, 2	na[a]	na[a]	na[a]	na[a]	48	−4.032
7, 2	na[a]	na[a]	na[a]	na[a]	53	−4.307
10, 2	na[a]	na[a]	na[a]	na[a]	60	−4.960
7, 20	na[a]	na[a]	na[a]	na[a]	55	−5.289
GO–MMT (Sphere–sphere)						
4, 2	0.25	-1.77×10^6	12	105.2	54	−2.837
7, 2	0.25	-5.50×10^5	11	55.1	55	−1.161
10, 2	0.25	-7.90×10^5	11	127.1	59	−1.457
7, 20	0.25	-1.12×10^6	na[a]	na[a]	na[a]	na[a]

[a]Values are not available.

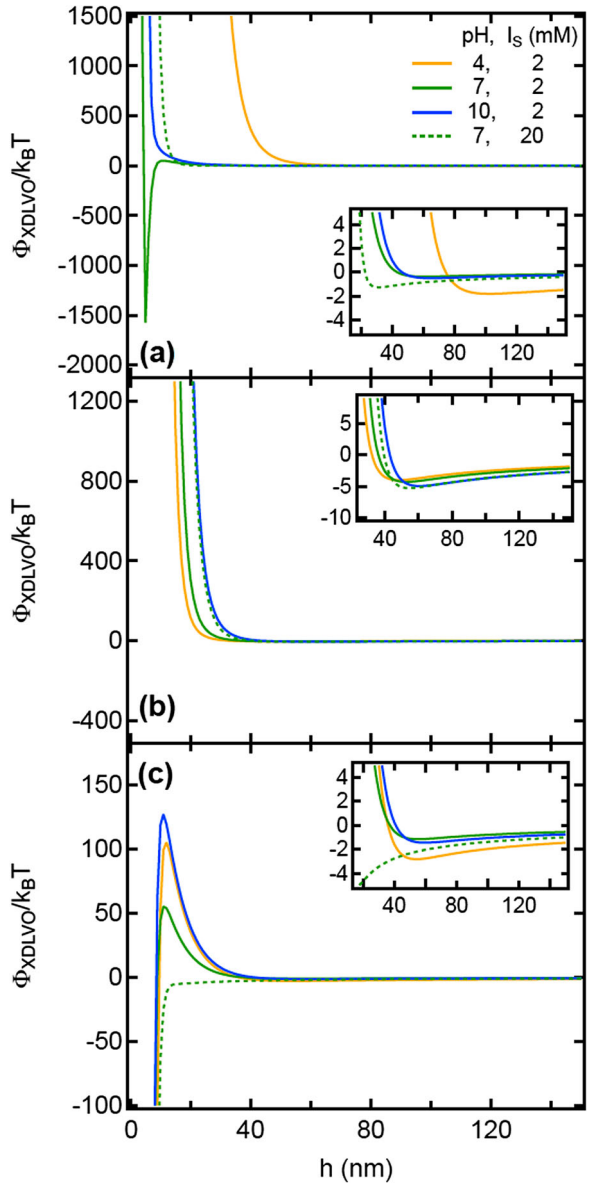

Figure 8. Predicted Φ_{XDLVO} profiles for: (a) GO–GO, (b) MMT–MMT, and (c) GO–MMT interactions, as a function of separation distance for various PBS solutions. Each figure insert highlights the corresponding Φ_{min2}.

4. Conclusions

Our results showed that GO attachment onto MMT and quartz sand was adequately described by the Freundlich isotherm equation. All attachment experiments were performed at 25°C. The results of kinetic study showed that attachment of GO on MMT and quartz sand surface was well interpreted by the pseudo-second-order kinetic model because of the low value of the Chi-square statistic and high correlation coefficient values. The results of pH effect showed that there was no significant change in MMT mass attached onto sand grains with increasing pH values from 7 to 10; therefore, the PBS solution pH for the attachment experiments was fixed at pH = 7. GO was found to be attached in greater amounts onto MMT than quartz sand. However, the attachment of GO onto quartz sand was shown a slight increase with the presence of MMT colloids. Moreover, the observed enhanced total GO attachment onto both quartz sand and MMT when they co-exist might decrease GO mobility in natural aquatic environments. It should be noted that the results of this study provide important basic information for the effectiveness of montmorillonite to remove GO from dilute aqueous solutions in columns packed with quartz sand. Finally, Lewis acid–base interactions played an important role in the total interaction energy, and certainly, successfully explained the hydrophobic interaction-mediated attachment of GO onto MMT and quartz sand.

Disclosure statement

No potential conflict of interest was reported by the authors.

Funding

This research has been supported by the State Scholarship Foundation ('IKY Fellowships of Excellence for Postgraduate Studies in Greece-Siemens Program') in the framework of the Hellenic Republic-Siemens Settlement Agreement.

References

[1] Shen Y, Fang Q, Chen B. Environmental applications of three-dimensional graphene-based macrostructures: adsorption, transformation, and detection. Environ Sci Technol. 2014;49:67–84.
[2] Bhattacharya M. Polymer nanocomposites-A comparison between carbon nanotubes, graphene, and clay as nanofillers. Materials (Basel). 2016;9:262.
[3] Compton OC. Nguyen ST. Graphene oxide, highly reduced graphene oxide, and graphene: versatile building blocks for carbon-based materials. Small. 2010;6:711–723.
[4] Dong S, Shi X, Gao B, et al. Retention and release of graphene oxide in structured heterogeneous porous media under saturated and unsaturated conditions. Environ Sci Technol. 2016;50:10397–10405.
[5] Chrysikopoulos C V, Sotirelis NP, Kallithrakas-Kontos NG. Cotransport of graphene oxide nanoparticles and kaolinite colloids in porous media. Transp Porous Media. 2017;119:181–204.
[6] Syngouna VI, Chrysikopoulos C V. Cotransport of clay colloids and viruses in water saturated porous media. Colloids Surf A Physicochem Eng Asp. 2013;416:56–65.
[7] Bellou MI, Syngouna VI, Tselepi MA, et al. Interaction of human adenoviruses and coliphages with kaolinite and bentonite. Sci Total Environ. 2015;517:86–95.
[8] Syngouna VI, Chrysikopoulos CV. Experimental investigation of virus and clay particles cotransport in partially

saturated columns packed with glass beads. J Colloid Interface Sci. 2015;440:140–150.
[9] Syngouna VI, Chrysikopoulos CV. Cotransport of clay colloids and viruses through water-saturated vertically oriented columns packed with glass beads: gravity effects. Sci Total Environ. 2016;545:210–218.
[10] Begg JD, Zavarin M, Zhao P, et al. Pu (V) and Pu (IV) sorption to montmorillonite. Environ Sci Technol. 2013;47:5146–5153.
[11] Feriancikova L, Xu S. Deposition and remobilization of graphene oxide within saturated sand packs. J Hazard Mater. 2012;235-235:194–200.
[12] Lanphere JD, Luth CJ, Walker SL. Effects of solution chemistry on the transport of graphene oxide in saturated porous media. Environ Sci Technol. 2013;47:4255–4261.
[13] Liu L, Gao B, Wu L, et al. Deposition and transport of graphene oxide in saturated and unsaturated porous media. Chem Eng J. 2013;229:444–449.
[14] Chowdhury I, Duch MC, Mansukhani ND, et al. Deposition and release of graphene oxide nanomaterials using a quartz crystal microbalance. Environ Sci Technol. 2014;48:961–969.
[15] Chowdhury I, Duch MC, Mansukhani ND, et al. Colloidal properties and stability of graphene oxide nanomaterials in the aquatic environment. Environ Sci Technol. 2013;47:6288–6296.
[16] Wu L, Liu L, Gao B, et al. Aggregation kinetics of graphene oxides in aqueous solutions: experiments, mechanisms, and modeling. Langmuir. 2013;29:15174–15181.
[17] Chowdhury I, Duch MC, Mansukhani ND, et al. Interactions of graphene oxide nanomaterials with natural organic matter and metal oxide surfaces. Environ Sci Technol. 2014;48:9382–9390.
[18] Qi Z, Zhang L, Wang F, et al. Factors controlling transport of graphene oxide nanoparticles in saturated sand columns. Environ Toxicol Chem. 2014;33:998–1004.
[19] Ren X, Li J, Tan X, et al. Impact of Al2O3 on the aggregation and deposition of graphene oxide. Environ Sci Technol. 2014;48:5493–5500.
[20] Fan W, Jiang X, Lu Y, et al. Effects of surfactants on graphene oxide nanoparticles transport in saturated porous media. J Environ Sci. 2015;35:12–19.
[21] Fan W, Jiang XH, Yang W, et al. Transport of graphene oxide in saturated porous media: effect of cation composition in mixed Na--Ca electrolyte systems. Sci Total Environ. 2015;511:509–515.
[22] Jian-Zhou H, Cheng-Cheng L, Deng-Jun W, et al. Biofilms and extracellular polymeric substances mediate the transport of graphene oxide nanoparticles in saturated porous media. J Hazard Mater. 2015;300:467–474.
[23] Liu L, Gao B, Wu L, et al. Effects of surfactant type and concentration on graphene retention and transport in saturated porous media. Chem Eng J. 2015;262:1187–1191.
[24] Sun Y, Gao B, Bradford SA, et al. Transport, retention, and size perturbation of graphene oxide in saturated porous media: effects of input concentration and grain size. Water Res. 2015;68:24–33.
[25] Xia T, Fortner JD, Zhu D, et al. Transport of sulfide-reduced graphene oxide in saturated quartz sand: cation-dependent retention mechanisms. Environ Sci Technol. 2015;49:11468–11475.
[26] Huang G, Guo H, Zhao J, et al. Effect of co-existing kaolinite and goethite on the aggregation of graphene oxide in the aquatic environment. Water Res. 2016;102:313–320.
[27] Chang K, Sun Y, Ye F, et al. Macroscopic and molecular study of the sorption and co-sorption of graphene oxide and Eu (III) onto layered double hydroxides. Chem Eng J. 2017;325:665–671.
[28] Peng S, Wu D, Ge Z, et al. Influence of graphene oxide on the transport and deposition behaviors of colloids in saturated porous media. Environ Pollut. 2017;225:141–149.
[29] Zhao J, Liu F, Wang Z, et al. Heteroaggregation of graphene oxide with minerals in aqueous phase. Environ Sci Technol. 2015;49:2849–2857.
[30] Sotirelis NP, Chrysikopoulos C V. Heteroaggregation of graphene oxide nanoparticles and kaolinite colloids. Sci Total Environ. 2017;579:736–744.
[31] Tombácz E, Szekeres M. Colloidal behavior of aqueous montmorillonite suspensions: the specific role of pH in the presence of indifferent electrolytes. Appl Clay Sci. 2004;27:75–94.
[32] Syngouna VI, Chrysikopoulos CV. Interaction between viruses and clays in static and dynamic batch systems. Environ Sci Technol. 2010;44:4539–4544.
[33] Sotirelis NP, Chrysikopoulos CV. Interaction between graphene oxide nanoparticles and quartz sand. Environ Sci Technol. 2015;49:13413–13421.
[34] Sanders RL, Washton NM, Mueller KT. Measurement of the reactive surface area of clay minerals using solid-state NMR studies of a probe molecule. J Phys Chem C. 2010;114:5491–5498.
[35] Van Olphen H, Fripiat J-J. Data handbook for clay materials and other non-metallic minerals: providing those involved in clay research and industrial application with sets of authoritative data describing the physical and chemical properties and mineralogical composition of the available reference materials. Oxford: Pergamon; 1979.
[36] Rong X, Huang Q, He X, et al. Interaction of pseudomonas putida with kaolinite and montmorillonite: a combination study by equilibrium adsorption, ITC, SEM and FTIR. Colloids Surfaces B Biointerfaces. 2008;64:49–55.
[37] Loveland JP, Ryan JN, Amy GL, et al. The reversibility of virus attachment to mineral surfaces. Colloids Surf A Physicochem Eng Asp. 1996;107:205–221.
[38] Xu S, Liao Q, Saiers JE. Straining of nonspherical colloids in saturated porous media. Environ Sci Technol. 2008;42:771–778.
[39] Chrysikopoulos C V, Aravantinou AF. Virus attachment onto quartz sand: role of grain size and temperature. J Environ Chem Eng. 2014;2:796–801.
[40] Mitropoulou PN, Syngouna VI, Chrysikopoulos CV. Transport of colloids in unsaturated packed columns: role of ionic strength and sand grain size. Chem Eng J. 2013;232:237–248.
[41] Zhou D, Abdel-Fattah AI, Keller AA. Clay particles destabilize engineered nanoparticles in aqueous environments. Environ Sci Technol. 2012;46:7520–7526.
[42] Ho Y-S. Review of second-order models for adsorption systems. J Hazard Mater. 2006;136:681–689.
[43] Anagnostopoulos VA, Manariotis ID, Karapanagioti HK, et al. Removal of mercury from aqueous solutions by malt spent rootlets. Chem Eng J. 2012;213:135–141.
[44] Katzourakis VE, Chrysikopoulos CV. Fitting the transport and attachment of dense biocolloids in One-dimensional porous media: ColloidFit. Groundwater. 2017;55:156–159.
[45] Freundlich HM. New conception in colloidal chemistry, colloid and capillary chemistry. London: Methuen and Co.; 1926.

[46] Chrysikopoulos CV, Syngouna VI. Attachment of bacteriophages MS2 and ΦX174 onto kaolinite and montmorillonite: extended-DLVO interactions. Colloids Surfaces B Biointerfaces. 2012;92:74–83.
[47] Shih C-J, Lin S, Sharma R, et al. Understanding the pH-dependent behavior of graphene oxide aqueous solutions: a comparative experimental and molecular dynamics simulation study. Langmuir. 2011;28:235–241.
[48] Mui J, Ngo J, Kim B. Aggregation and colloidal stability of commercially available Al2O3 nanoparticles in aqueous environments. Nanomaterials. 2016;6:90.
[49] Van Olphen H. An introduction to clay colloid chemistry. Soil Sci. 1964;97:290.
[50] Johnston CT, Tombácz E. Surface chemistry of soil minerals. In: Dixon JB, Schulze DG, editors. Soil mineralogy with environmental applications. Madison, WI: Soil Science Society of America; 2002. p. 37–67.
[51] Delhorme M, Labbez C, Caillet C, et al. Acid- base properties of 2: 1 clays. I. Modeling the role of electrostatics. Langmuir. 2010;26:9240–9249.
[52] Verwey EJW, Overbeek JThG. Theory of the stability of lyophobic colloids: The interaction of sol particles having an electric double layer. Amsterdam: Elsevier. 1948.
[53] Stoller MD, Park S, Zhu Y, et al. Graphene-based ultracapacitors. Nano Lett. 2008;8:3498–3502.
[54] Leroy P, Tournassat C, Bizi M. Influence of surface conductivity on the apparent zeta potential of TiO2 nanoparticles. J Colloid Interface Sci. 2011;356:442–453.
[55] Zuccaro L, Krieg J, Desideri A, et al. Tuning the isoelectric point of graphene by electrochemical functionalization. Sci Rep. 2015;5:11794–11798.
[56] Shih C-J, Wang QH, Lin S, et al. Breakdown in the wetting transparency of graphene. Phys Rev Lett. 2012;109:176101.
[57] Yu S, Wang X, Zhang R, et al. Complex roles of solution chemistry on graphene oxide coagulation onto titanium dioxide: batch experiments, spectroscopy analysis and theoretical calculation. Sci Rep. 2017;7:39625.
[58] McAtee Jr JL, Henslee W. Electron-microscopy of montmorillonite dispersed at various pH. Am Mineral J Earth Planet Mater. 1969;54:869–874.
[59] Norrish K. The swelling of montmorillonite. Discuss Faraday Soc. 1954;18:120–134.
[60] Karnland O, Olsson S, Nilsson U, et al. Experimentally determined swelling pressures and geochemical interactions of compacted Wyoming bentonite with highly alkaline solutions. Phys Chem Earth Parts A/B/C. 2007;32:275–286.
[61] García-García S, Degueldre C, Wold S, et al. Determining pseudo-equilibrium of montmorillonite colloids in generation and sedimentation experiments as a function of ionic strength, cationic form, and elevation. J Colloid Interface Sci. 2009;335:54–61.
[62] Yoshida T, Suzuki M. Effects of humic acid on migration of montmorillonite and alumina colloid in a quartz sand column. Colloids Surfaces A Physicochem Eng Asp. 2008;325:115–119.
[63] Delgado A, Gonzalez-Caballero F, Bruque JM. On the zeta potential and surface charge density of montmorillonite in aqueous electrolyte solutions. J Colloid Interface Sci. 1986;113:203–211.
[64] Tombacz E, Libor Z, Illes E, et al. The role of reactive surface sites and complexation by humic acids in the interaction of clay mineral and iron oxide particles. Org Geochem. 2004;35:257–267.
[65] Sposito G. The surface chemistry of soils. New York: Oxford University Press; 1984.
[66] Shen C, Li B, Huang Y, et al. Kinetics of coupled primary- and secondary-minimum deposition of colloids under unfavorable chemical conditions. Environ Sci Technol. 2007;41:6976–6982.
[67] Yoon R-H, Flinn DH, Rabinovich YI. Hydrophobic interactions between dissimilar surfaces. J Colloid Interface Sci. 1997;185:363–370.